Characterization of Stimulation Artifact Behavior in Simultaneous Electrocorticography Grid Stimulation and Recording

Jeffrey Lim[1], Po T. Wang[1], Alireza K. Bidhendi[2], Omid M. Arasteh[2], Susan J. Shaw[3], Michelle Armacost[3], Hui Gong[3], Charles Y. Liu[3], Payam Heydari[2], An H. Do[4], and Zoran Nenadic[1,2]

***Abstract*— Bi-directional brain-computer interfaces (BCIs) require simultaneous stimulation and recording to achieve closed-loop operation. It is therefore important that the interface be able to distinguish between neural signals of interest and stimulation artifacts. Current bi-directional BCIs address this problem by temporally multiplexing stimulation and recording. This approach, however, is suboptimal in many BCI applications. Alternative artifact mitigation methods can be devised by investigating the mechanics of artifact propagation. To characterize stimulation artifact behaviors, we collected and analyzed electrocorticography (ECoG) data from eloquent cortex mapping. Ratcheting and phase-locking of stimulation artifacts were observed, as well as dipole-like properties. Artifacts as large as ±1,100 μV appeared as far as 15-37 mm away from the stimulating channel when stimulating at 10 mA. Analysis also showed that the majority of the artifact power was concentrated at the stimulation pulse train frequency (50 Hz) and its super-harmonics (100, 150, 200 Hz). Lower frequencies (0-32 Hz) experienced minimal artifact contamination. These findings could inform the design of future bi-directional ECoG-based BCIs.**

I. INTRODUCTION

Electrocorticography (ECoG)-based brain-computer interfaces (BCIs) have shown promising results in restoring functions to those with severe motor deficits [1], [2]. These systems achieve closed-loop operation by utilizing visual feedback. This, however, may be suboptimal for movement restoration, where somatosensory feedback plays a crucial role. By endowing BCIs with somatosensory feedback, movement and sensation are thus integrated in a biomimetic fashion, which may lead to more intuitive BCI operation. In addition, these so-called bi-directional BCIs [3], [4] could outperform those that are solely reliant on visual feedback.

For individuals lacking sensation, somatosensory feedback can be elicited by delivering electrical stimulation to the primary sensory cortex. The utility of this approach has already been demonstrated in a microelectrode-based BCI [5]. Similarly, the ability to elicit artificial sensation through ECoG grid cortical stimulation has recently been reported in [6], although not in the context of BCI control. Regardless of the signal recording modality, the presence of strong stimulation artifacts remains a major technical hurdle for bi-directional BCI operation. These artifacts can overwhelm the neural signals of interest and saturate analog recording front-ends. Improving amplifier linearity cannot singlehandedly avoid the front-end saturation, as the artifact amplitude is comparable with the nominal supply voltage used in ultra-low-power (ULP) amplifiers. As ULP analog front-ends are the backbone of future fully implantable BCIs [3], [4], efficient strategies for artifact suppression must be developed.

State-of-the art microelectrode-based, bi-directional BCIs mitigate this problem by temporally multiplexing neural recording and electrical stimulation [5], [7]. While this strategy may be sufficient for providing intermittent feedback, it is inadequate in applications where continuous feedback is needed. In addition, it imposes constraints on BCI decoding algorithms and the choice of stimulation parameters. An alternative approach is to understand how artifacts propagate through cortical tissues and use this knowledge to devise artifact suppression strategies. In general, the artifact propagation depends on the distance between stimulating and recording electrodes, their relative orientation, the electrical properties of the tissue and tissue-electrode interface, as well as the intensity and spectral properties of stimulation signals. Some of these factors have been incorporated in the design of ECoG-based, bi-directional BCI prototypes [3], [4]; however, comprehensive experimental studies characterizing ECoG stimulation artifact propagation are generally lacking.

Motivated by this knowledge gap, we collected ECoG data from a subject undergoing cortical electrostimulation for clinical purposes. We then characterized artifacts across multiple recording and stimulating electrode locations and orientations, as well as a range of stimulation amplitudes. Our analysis may inform the design of future fully implantable, bi-directional, ECoG-based BCIs.

II. METHODS

A. Stimulation Procedure

The study was approved by the Institutional Review Board of the Rancho Los Amigos National Rehabilitation Center and the University of California, Irvine. The data were collected during a language cortex mapping procedure performed as part of the surgical evaluation of a 39-year-old epilepsy patient. ECoG grids (Integra LifeSciences, Plainsboro NJ) were implanted as shown in Fig. 1, where all electrodes were made of platinum. Stimulating channels consisted of pairs of adjacent electrodes. The stimulation waveform was a 50 Hz biphasic square pulse train of current with a duty cycle of 200 μs. These pulse trains were delivered using a Natus® Quantum™ cortical stimulator (Natus

Supported by National Science Foundation (Award # 1446908, 1646275)

[1]Dept. of Biomedical Engineering, University of California Irvine (UCI), Irvine, CA 92697, USA {limj4,ptwang,znenadic}@uci.edu

[2]Dept. of Electrical Engineering and Computer Science, UCI, Irvine, CA 92697, USA {akarimib,omalekza,payam}@uci.edu

[3]Rancho Los Amigos National Rehabilitation Center, Downey, CA, USA

[4]Dept. of Neurology, UCI, Irvine, CA 92697, USA and@uci.edu

Medical Incorporated, Pleasanton CA) for approximately 5 seconds at 2, 4, 6, 8, 10 and occasionally 12 mA. This sequence of current amplitudes was delivered twice for each stimulating channel. ECoG data were captured at 512 Hz sampling frequency. Electrode recordings were referenced with respect to LTG19 and ground was located at LTG20 (Fig. 1).

B. Data Analysis

A zero-phase, first-order, Butterworth high-pass filter (>1.5 Hz) was first applied to the time series. The five second stimulation epochs were then segmented. Data from the stimulating pair of electrodes could not be used during these epochs since their signals were clipped due to amplifier saturation. For the remaining electrodes, the amplitudes of individual stimulation artifacts were calculated. There were ∼250 such artifacts per epoch, and they were characterized by their median value. These median values were spatially interpolated and color-coded to generate spatial distribution maps of artifact amplitudes.

The interpretation of these data was aided by defining a hypothetical ULP amplifier saturation region based on an implantable bi-directional BCI prototype [4]. Assuming a supply voltage of 2.2 V and a gain of 66 dB, we calculated a saturation limit of ±1,100 μV. This value yielded a contour in the spatial distribution map, with its interior defining the saturation region. The extent of the saturation region was then characterized by calculating the maximum distance between the mid-point of each stimulation channel and the saturation contour.

For the frequency domain analysis, the stimulation epochs were divided into 10 non-overlapping segments. A Fourier transform was performed on these 500-ms-long data segments and their power spectral densities (PSDs) were calculated. The same procedure was repeated for five seconds of non-stimulation data immediately preceding each stimulation epoch. The Kolmogorov-Smirnov (KS) test was used to determine whether the differences in the PSDs of stimulation and non-stimulation data were statistically significant. In addition, to characterize the stimulation interference at each frequency, we calculated the interference index:

$$I(f) = \frac{1}{2}\log\frac{\sigma_t^2(f)}{\sigma_{on}(f)\sigma_{off}(f)} \quad (1)$$

where σ_{on}^2 and σ_{off}^2 are the variances of the PSDs of stimulation and non-stimulation data, respectively, calculated over the 10 segments, and σ_t^2 is the total variance of the combined PSDs. Note that (1) is a variant of the deflection coefficient [8] that has been modified to account for overlapping means and unequal variances [9].

III. RESULTS

1) Ratcheting Effect: Inspection of the data before high-pass filtering revealed large deviations in the baseline both on the stimulating electrodes and other electrodes nearby the stimulating channel (Fig. 2). The effect appeared to accumulate between stimulating epochs as well as scale with

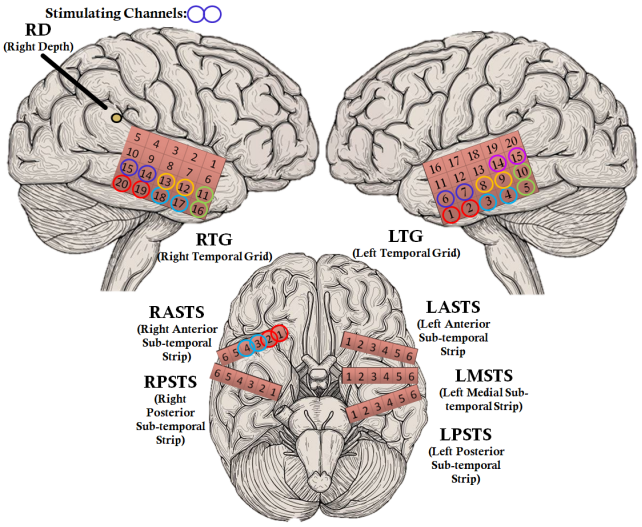

Fig. 1. Placement of electrocorticography grids (not to scale). Pairs of colored circles indicate individual stimulating channels.

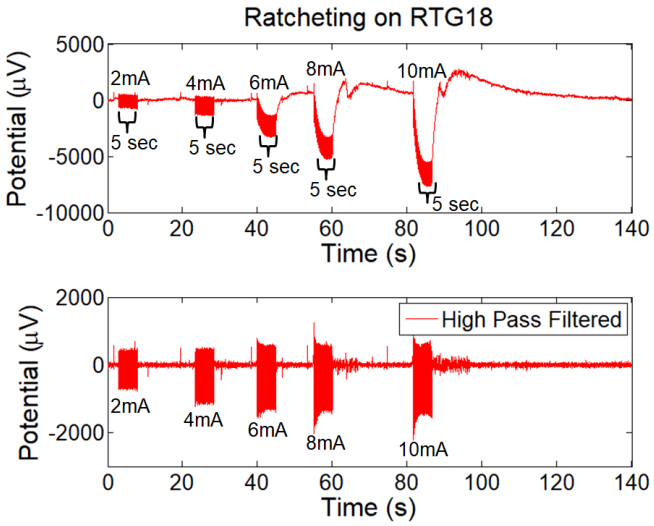

Fig. 2. Top plot is a representative example of unfiltered data with baseline deviations (ratcheting). Stimulating channel is located adjacently on RTG19-20. Bottom plot demonstrates the elimination of the ratcheting effect by high pass filtering.

stimulation amplitude. It was also strong enough to drive the signals on the stimulating channel above the data acquisition system's saturation limit (±8.7 mV). The effect of ratcheting was removed by high-pass filtering (Fig. 2).

2) Phase-Locking of Stimulation Artifacts: Artifact peaks appearing on one electrode occurred within ∼2 ms (1 sample) of artifact peaks on other electrodes (Fig. 3). These peaks also occur approximately 20 ms apart, which matches the 50 Hz frequency of the original stimulation pulse train.

3) Distribution of Stimulation Artifact Amplitude: The spatial distribution of median stimulation artifact amplitudes followed a dipole distribution (Fig. 4), with artifact size proportional to the stimulation amplitude. The worst-case analysis was performed for each stimulation epoch by calculating the extent of the saturation region and the stimulation

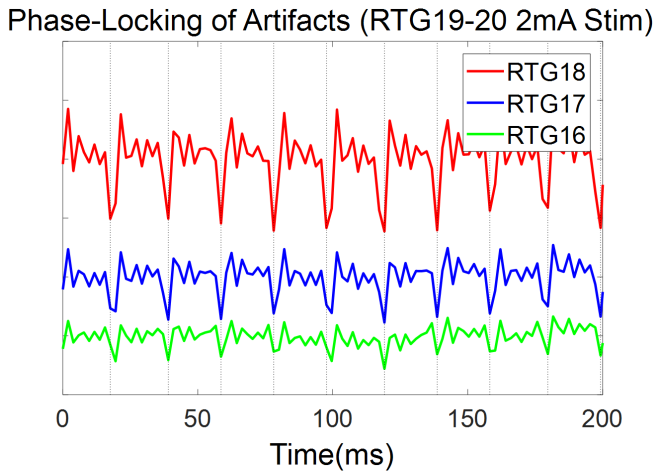

Fig. 3. A representative example of phase-locking of stimulation artifacts across adjacent electrodes.

TABLE I
CHARACTERIZATION OF WORST-CASE ARTIFACT SPREAD

stimulation channel	extent of saturation region (mm)	stimulation amplitude (mA)
RTG11-16	41.21	6
RTG12-13	27.62	10
RTG14-15	24.22	10
RTG17-18	17.14	10
RTG19-20	32.37	10
LTG1-2	18.85	10
LTG3-4	19.50	10
LTG5-10	18.76	12
LTG6-7	36.50	10
LTG8-9	20.73	12
LTG14-15	15.89	12

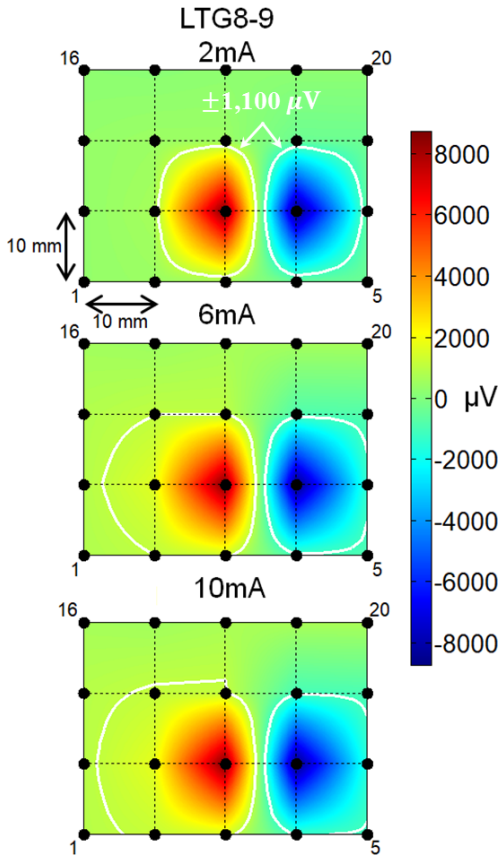

Fig. 4. Distribution of artifact amplitudes in LTG resulting from stimulation applied at LTG8-9 for different stimulation strengths. The interior of the white contours indicates the hypothetical ULP amplifier saturation region.

amplitude at which it occurred (Table I). The saturation region generally grew monotonically with stimulation amplitude, which is consistent with dipole behavior. An exception occurred at stimulating channel RTG11-16 where the largest saturation region was observed at 6 mA.

4) Frequency Domain Analysis: Fig. 5 shows an example of the impact of stimulation artifacts in the frequency domain. For the stimulating channel RTG19-20, the worst-case interference is observed at the adjacent electrode RTG18 for a stimulating current of 10 mA. The interference index showed that the strongest interference occurred around 50 Hz and its super-harmonics (100, 150, 200 Hz), which concurs with the stimulation pulse train frequency. Conversely, frequencies from 0 to 32 Hz showed lower interference. These results are corroborated by the KS test, which shows that the two PSD populations were generally not significantly different in the 0-32 Hz band.

IV. DISCUSSION

Our analysis has revealed a few notable behaviors of artifacts in ECoG grid stimulation. Some of these could be exploited for the development of artifact suppression techniques, while others impose constraints on BCI designs.

The ratcheting effect [10] likely results from a loss of charge to Faradaic processes. When current is delivered through the stimulating channel, the initial charge generated by the first phase of the biphasic pulse is stored in the bilayer capacitance formed at the interface between the electrode and the brain tissue. Any remaining charge is consumed via Faradaic processes, which for platinum electrodes occurs via hydrogen adsorption to the electrode surface. The second phase of the biphasic pulse reverses the charging of the bilayer capacitance, but since some of the charge from the first phase was consumed in Faradaic processes, there is an overcorrection. If another biphasic pulse arrives before this overcorrection discharges, the ratcheting accumulates. The time constant for this discharge appears to be on the order of seconds (see Fig. 2), which is problematic since the stimulation pulse train frequency is faster than the rate at which electrode-tissue interface can discharge. BCI designs should include charge recovery mechanisms to minimize or eliminate these transient charge accumulations.

The phase-locking of artifacts across electrodes suggests that stimulation currents are primarily transferred via volume conduction through a resistive medium (likely a combination of brain tissue and cerebrospinal fluid), and that impedances across channels are approximately equal. This insight could be used to model artifact propagation in the framework of dynamical system theory. This model could also shed a light on the electrical properties of underlying tissues.

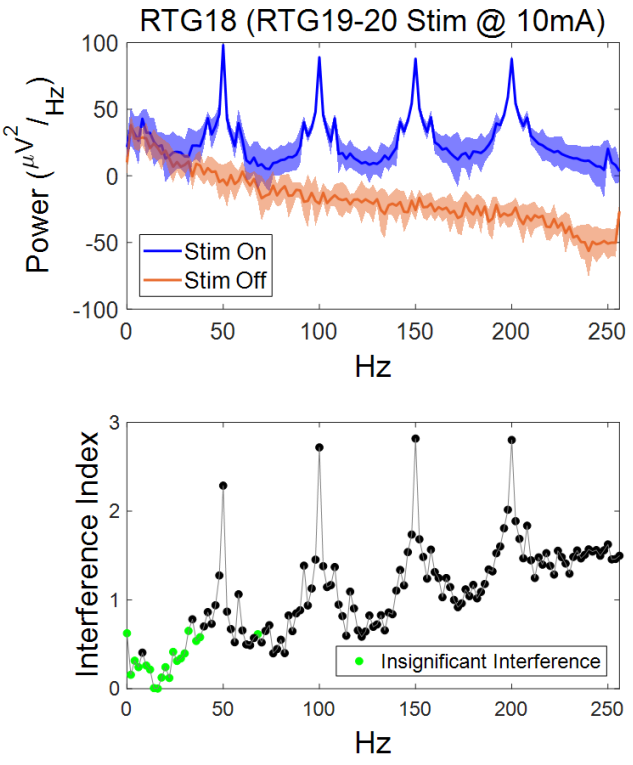

Fig. 5. Top graph shows the average PSD of recordings on RTG18 during epochs with and without stimulation. Stimulation amplitude was 10 mA applied at RTG19-20. Shaded regions represent ± 1 standard deviation around the mean. Bottom graph indicates the degree of interference [as calculated by (1)] as a function of frequency. Green points indicate frequencies at which there was no significant difference (KS test, p-value=0.01) between the PSDs with and without stimulation.

The artifact spatial maps exhibited dipole-like qualities in that the spread was greatest in the direction co-linear with the dipole moment. The spread also increased monotonically with the stimulation amplitude. An exception was channel RTG11-16 at 6 mA, for which an additional saturation contour emerged away from the stimulation channel. Nonlinear, switch-like behavior could explain this anomaly in that specific stimulation amplitudes could have activated alternative conduction pathways in the brain. Nevertheless, these findings suggest that a dipole model may yield accurate predictions regarding the spatial distribution of stimulation artifacts.

The amplifier saturation region depends on parameters such as the amplifier gain and supply voltage, and maps like the one in Fig. 4 could provide additional design specifications for ULP analog front-ends. For example, the tolerance toward stimulation artifacts could be improved by reducing the gain of the amplifier or increasing its supply voltage, but at the cost of compromising signal quality or reducing the battery life, respectively. Another option is to simply place the recording electrodes sufficiently far from the stimulating channel. There is, however, a limit as to how far recording and stimulating electrodes can be separated since they must cover physiologically relevant brain areas. For electrodes outside the saturation region, artifacts can be suppressed and neural information recovered by applying array signal processing techniques [11].

Our frequency domain analysis suggests that most of the artifact power is distributed at and above the stimulation pulse train frequency. Therefore, one could potentially keep the recording band of a bi-directional BCI clear by increasing the frequency of the stimulation pulse train. ECoG-based cortical stimulation with frequencies up to 500 Hz have been found capable of eliciting somatosensation [6]. This is well beyond the upper γ frequency which plays an important role in movement control [12], and has been identified as a primary band for ECoG-based BCIs.

Since our study is a case report, data from additional subjects need to be analyzed to ensure that these results are generalizable. Another limiting factor in our study is the relatively low sampling rate (512 Hz), which precluded analyzing the array's response from a dynamical system's perspective with a sufficient resolution. Our future efforts will therefore be directed toward collecting additional data with higher sampling rates.

References

[1] W Wang, JL Collinger, AD Degenhart, EC Tyler-Kabara, AB Schwartz, DW Moran, DJ Weber, B Wodlinger, RK Vinjamuri, RC Ashmore, et al. An electrocorticographic brain interface in an individual with tetraplegia. *PloS ONE*, 8(2):e55344, 2013.

[2] MJ Vansteensel, EGM Pels, MG Bleichner, MP Branco, T Denison, ZV Freudenburg, P Gosselaar, S Leinders, TH Ottens, M Van Den Boom, et al. Fully implanted braincomputer interface in a locked-in patient with als. *New England Journal of Medicine*, 375(21):2060–2066, 2016.

[3] S Stanslaski, P Cong, D Carlson, W Santa, R Jensen, G Molnar, WJ Marks, A Shafquat, and T Denison. An implantable bi-directional brain-machine interface system for chronic neuroprosthesis research. In *Proc. 31st Ann. Int. Conf. IEEE EMBS*, pages 5494–5497, 2009.

[4] AG Rouse, SR Stanslaski, Peng Cong, RM Jensen, Pedram Afshar, Dave Ullestad, R Gupta, GF Molnar, DW Moran, and TJ Denison. A chronic generalized bi-directional brain–machine interface. *J. Neural Eng.*, 8(3):036018, 2011.

[5] S Flesher, J Downey, J Collinger, S Foldes, J Weiss, E Tyler-Kabara, S Bensmaia, A Schwartz, M Boninger, and R Gaunt. Intracortical microstimulation as a feedback source for brain-computer interface users. In *Brain-Computer Interface Research*, pages 43–54. Springer, 2017.

[6] SV Hiremath, EC Tyler-Kabara, JJ Wheeler, DW Moran, RA Gaunt, JL Collinger, ST Foldes, DJ Weber, W Chen, ML Boninger, et al. Human perception of electrical stimulation on the surface of somatosensory cortex. *PloS ONE*, 12(5):e0176020, 2017.

[7] JE O'Doherty, MA Lebedev, PJ Ifft, KZ Zhuang, S Shokur, H Bleuler, and MAL Nicolelis. Active tactile exploration using a brain–machine–brain interface. *Nature*, 479(7372):228, 2011.

[8] SM Kay. *Fundamentals of Statistical Signal Processing: Detection Theory*. Prentice-Hall, Englewood Cliffs, NJ, 1998.

[9] Z Nenadic. Information discriminant analysis: Feature extraction with an information-theoretic objective. *IEEE T. Pattern Anal.*, 29(8):1394–1407, 2007.

[10] DR Merrill, M Bikson, and JGR Jefferys. Electrical stimulation of excitable tissue: design of efficacious and safe protocols. *Journal of neuroscience methods*, 141(2):171–198, 2005.

[11] S-C Wu, AL Swindlehurst, PT Wang, and Z Nenadic. Projection vs. prewhitening for eeg interference suppression. *IEEE T. Bio-med. Eng.*, 59(5):1329–1338, 2012.

[12] Po T Wang, Colin M McCrimmon, Christine E King, Susan J Shaw, David E Millett, Hui Gong, Luis A Chui, Charles Y Liu, Zoran Nenadic, and An H Do. Characterization of electrocorticogram high-gamma signal in response to varying upper extremity movement velocity. *Brain Structure and Function*, 222(8):3705–3748, 2017.